TELKOMNIKA Telecommunication, Computing, Electronics and Control
Vol. 22, No. 5, October 2024, pp. 1280∼1292
ISSN: 1693-6930, DOI: 10.12928/TELKOMNIKA.v22i5.26347

ANN-based design of miniaturized circular dual-band 4×4 MIMO antenna for 28/38 GHz 5G mmWave applications

Lahcen Sellak[1], Asma Khabba[2], Samira Chabaa[1,2], Saida Ibnyaich[2], Atmane Baddou[1], Abdelouhab Zeroual[2], Tole Sutikno[3]
[1]LISAD Research Laboratory, Department of Industrial Engineering, National School of Applied Sciences, Ibn Zohr University, Agadir, Morocco
[2]I2SP Research Team, Department of Physics, Faculty of Sciences, Cadi Ayyad University, Marrakech, Morocco
[3]Department of Electrical Engineering, Faculty of Industrial Technology, Universitas Ahmad Dahlan, Yogyakarta, Indonesia

Article Info

Article history:

Received May 11, 2024
Revised Jun 7, 2024
Accepted Jul 12, 2024

Keywords:

5G technologies
Antenna
Artificial neural network
Millimeter wave
Multiple input multiple output

ABSTRACT

This paper introduces an innovative approach to design an extremely compact circular dual-band antenna suitable for 28/38 GHz 5G mmWave communications. Leveraging artificial neural network (ANN) and specially, multilayer perceptron (MLP) architecture, the suggested antenna's dimensions, which allow it to resonate across both frequencies, are predicted. The proposed circular patch antenna, featuring strategically placed rectangular and circular slots in the patch and the ground plane, attains a remarkable frequency range of 3 and 2 GHz for the initial resonant frequency of 28 GHz and the subsequent resonant frequency of 38 GHz bands, respectively. With maximal gains of 4.5 and 7 dB at the corresponding resonance frequency, respectively, the antenna also exhibits high efficiency. Remarkably, the dimensions of the individual antenna element are compact, measuring $4\times6\times0.8$ mm^3, showcasing a notable decrease in physical footprint. Furthermore, the single antenna seamlessly transforms into a 4×4 multiple input multiple output (MIMO) antenna occupying a total volume of $16\times16\times0.8$ mm^3, showcasing superior isolation and good diversity performance. This research not only contributes significantly to advancing miniaturized dual-band antennas tailored for 5G mmWave applications but also underscores the effectiveness of ANN, particularly MLP architecture, in optimizing antenna designs. The proposed antenna, with its small form factor, stands out as a promising solution for new generation 5G communication systems.

Corresponding Author:

Lahcen Sellak
LISAD Research Laboratory, Department of Industrial Engineering, National School of Applied Sciences
Ibn Zohr University
Agadir, Morocco
Email: lahcen.sellak@edu.uiz.ac.ma

1. INTRODUCTION

The advent of fifth generation (5G) technology represents an important moment in the evolution of wireless communication systems, bringing in a future that promises surpassing data speeds, ultra-low latency, and connection that extends beyond network borders. This 5G of mobile networks is predicted to disrupt a variety of sectors by allowing disruptive applications ranging from augmented reality and self-driving cars to widespread machine-type communications [1]. Unlocking the full potential of 5G, however, requires the resolution of several challenges, with the forefront of these efforts being dedicated to advancements in antenna design. The use of millimeter-wave (mmWave) frequencies, notably in the bands of 28 GHz and 38 GHz, is a critical feature of 5G technology. Because of its wide bandwidth, the mmWave spectrum is a major enabler for satisfying the ever-increasing needs for data transfer and connection [2]. Nonetheless, the use of high frequencies poses other issues, such as increased air absorption and sensitivity to obstacles. Despite these challenges, the compelling promise of delivering extraordinary data rates and minimal latency has fueled major research and development projects focused at applying the enormous potential of mmWave frequencies for 5G applications [3]–[5].

Recognizing the strategic importance of these frequencies, regulatory agencies like the federal communication commission (FCC) have specified pioneer bands for 5G wireless networks around 28 GHz and 38 GHz, including ranges like 26.5-29.5 GHz, 27.5-28.35 GHz, and 37-40 GHz. This allocation is consistent with the overall aim of providing operators with dependable connection that includes high bandwidth, increased data speeds, and low latency. Within the regulatory frameworks of both the FCC and the European Union (EU), various frequency bands have been allocated for the deployment of 5G networks, primarily falling within the ka-band spectrum (26–40 GHz). These bands include foundational ones such as the 26 GHz band (24.25–27.5 GHz), the 28 GHz band (27.5–28.35 GHz), and the 38 GHz band (37–40 GHz), as well as supplementary bands like the 24 GHz band (24.25–24.45 GHz, 24.75–25.25 GHz), the 29 GHz band (29.1–29.25 GHz), and the 32 GHz band (31.4–33.8 GHz) [6], [7]. The incorporation of the multiple input multiple output (MIMO) antenna system endowed with broadband characteristics stands as a pivotal component in creating the communication architecture of 5G wireless networks [8]. This technological facet plays a crucial role in elevating data rates, enhancing spectrum efficiency, and augmenting channel capacity. Leveraging the intricacies of the multipath channel, this MIMO antenna configuration achieves these advancements without necessitating an escalation in antenna feeding power. This underscores the indispensability of MIMO antennas in the architecture of 5G networks, providing a pathway to achieve higher data rates while concurrently optimizing spectral resources and channel capacity [9]. A variety of literature study has dug into the examination of MIMO antennas working at 28/38 GHz, highlighting their critical significance in 5G mmWave communication. A notable example is shown in Rafique *et al.* [10], where researchers propose a unique planar MIMO antenna array with an inset fed layout precisely built for 5G applications at 28 GHz and 38 GHz. It is notable for its small size, measuring $41.5\times10\times0.8$ mm^3, and it has excellent bandwidths of 1.39 GHz and 3.33 GHz for the corresponding bands of frequency. The maximum gain is 5.7 dB. Marzouk *et al.* [11], a MIMO antenna array comprising four elements and occupying an area of 110×55 mm^2 was created. The attainment of a dual-band response was realized through utilizing slots shaped like inverted I's was integrated in the primary patch. It's demonstrates commendable port isolation and achieves maximum gains of 7.95 dB and 8.27 dB in the respective frequency bands. Raheel *et al.* [12], a 4×4 MIMO antenna is introduced for 5G applications. The system, operational at both 28 GHz and 38 GHz frequencies, showcases an impressive minimum port isolation of 28 dB. The observed gains are 7.1 dB and 7.9 dB at 28 GHz and 38 GHz, respectively. Farahat and Hussein [13] introduces a MIMO antenna designed by the author with a dimension of 79.4×9.65 mm^2. It achieves a notable maximum gain of 9 dB and exhibits bandwidths of 3.42 GHz and 1.45 GHz for the respective frequency bands. *Usman et al.* [14], a small dual-port individual-element MIMO antenna functioning at a frequency of 28 GHz is introduced. The antenna features a total size of $33\times27.5\times0.76$ mm^3, exhibiting a bandwidth of 0.4 GHz and achieving a peak gain of 6.9 dB at 28 GHz. The design approach utilized in the references mentioned adheres to conventional methods, featuring a thorough parametric study as a fundamental aspect of the design process. It is important to acknowledge that this traditional method, while comprehensive, may demand more time and effort. An alternative to this approach involves leveraging artificial intelligence methods, such as ANN [15]–[17], radial basis function neural networks (RBFNN) [18]–[20], and adaptive neuro-fuzzy inference systems (ANFIS) [21]. These intelligent methods offer the potential to streamline the design process and enhance efficiency by leveraging computational capabilities and learning algorithms.

This paper delves into the intricate realm of mmWave communication, focusing on crafting a 4×4 MIMO antenna array optimized specifically for the challenging 28 GHz and 38 GHz bands. Leveraging the power of artificial neural network techniques, our approach aims to tackle the complexities associated with antenna design in the mmWave spectrum, providing insights into the advancements crucial for harnessing the full potential of 5G mmWave technology.

This paper is structured to provide a thorough exploration of the suggested circular 4×4 MIMO antenna for 5G applications. Beginning with an introduction, section 2 delves into the design and performance of the single antenna, offering a detailed discussion of the methodology and results. Section 3 focuses on presenting the collective performance attributes of the MIMO antenna. In section 4, a comparative study with other relevant works is conducted, highlighting the uniqueness and superiority of the proposed design. The paper concludes in the last section.

2. SUGGESTED SINGLE ANTENNA DESIGN AND METHOD

2.1. Layout of the proffered antenna

The proffered antenna's layout is displayed in Figures 1(a) and (b) for both top and back views. As can be seen in Figure 1(a), the antenna features a circular radiating patch with three inserted slots: two rectangular slots and one circular slot. The antenna operates using a 50 Ω microstrip transmission line, integrating two gaps between the microstrip conductor and the radiating patch. It is crafted on a Rogers RT5880 substrate, known for its advantageous attributes such as a dielectric constant (ϵ_r) of 2.2, a minimal loss tangent of 0.0009, and a thickness of 0.8 mm. As illustrated in Figure 1(b), the back of the substrate has a ground plane made of metal, featuring an etched circular slot alongside the rectangular slot, providing structural stability. Remarkably, the antenna maintains compact dimensions of $W_{sub} \times L_{sub} \times 0.8$ mm^3, with specific parameter values outlined in Table 1. Noteworthy is that the antenna's dimensions were optimized using an ANN structure, and subsequently, these dimensions were subjected to simulation using both the high-frequency structure simulator (HFSS) and computer simulation technology (CST) software for thorough analysis.

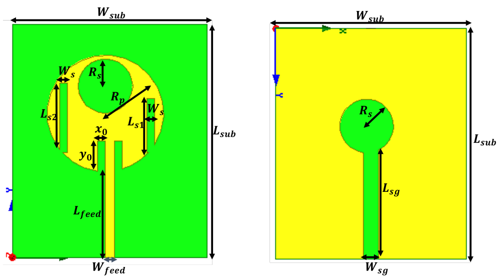

(a) (b)

Figure 1. Structure of the highlighted dual-frequency antenna design: (a) top view (b) back view

Table 1. Antenna's physical dimensions

Parameter	Value (mm)	Parameter	Value (mm)
R_p	1.4872	H_{sub}	0.8
L_{sub}	6	L_{sg}	3.0862
W_{sub}	5	W_{sg}	0.4047
W_{feed}	0.23	x_0	0.2
L_{feed}	2.26	y_0	0.78
L_{s1}	1.4876	W_S	0.1986
L_{s2}	1.8876	R_s	0.7239

2.2. Proposed method

The inception of mathematical modeling for understanding the human brain traces back to 1943, marked by the pioneering contributions of W. M. Culloch and W. Pitts [22]. According to their model, the neural impulse arises from the elementary computation of individual neurons, while cognition emerges from the collective behavior of interconnected neural networks [23]. An ANN is a system of parts that are linked together, termed "neurons" in homage to its biological inspiration, where each neuron executes a basic function, and their cumulative interplay displays complicated global characteristics. Operating independently, each neuron contributes to a system with massive parallelism, data is stored within a dispersed fashion using synaptic coefficients or activation functions. Notably, ANNs possess the capacity to acquire knowledge from their surroundings, enhancing performance through a learning process. During this research, we focus on supervised learning, leveraging input-output data obtained from simulating 219 antennas. The architecture of a typical

ANN includes input, hidden, and output layers. The network's neurons in each layer are interconnected, facilitating the learning process. A multilayer perceptron (MLP) neural network, illustrated in Figure 2, involves input, hidden, and output layers with interconnected neurons. The dimensions of the antenna structure were optimized using an ANN structure, and the obtained dimensions were subsequently simulated using renowned electromagnetic simulators like HFSS and CST software for comprehensive analysis. Activation functions such as logsig, tansig, and purlin are utilized in the neural network layers, with the selection of the appropriate activation function warranting further study. During the learning phase, the primary objective is to ascertain a number of training procedures are used to determine the ideal synapses weights as well as biases. These algorithms encompass resilient backpropagation (RP), Polak-Ribiere conjugate gradient (CGP), Bayesian regularization (BR), conjugate gradient with Fletcher-Peeves (CGF), Levenberg-Marquardt (LM), scaled conjugate gradient (SCG), one-step secant (OSS) and Powell-Beale conjugate gradient (CGB). Their effectiveness is assessed to pinpoint the most suitable algorithm, aimed at reducing the discrepancy between desired and predicted outputs.

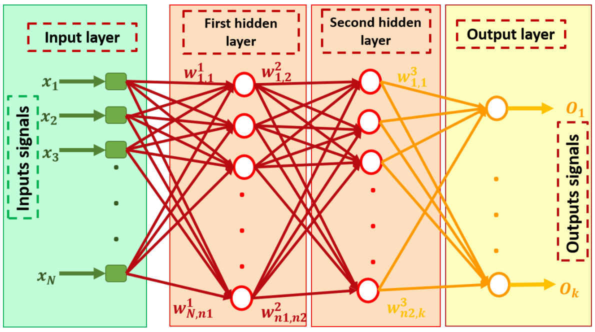

Figure 2. Structure of artificial neural network

2.3. Development and performance evaluation of the ANN model

In the endeavor to enhance the ANN architecture for forecasting the dimensions of the proposed dual-band antenna, an extensive dataset comprising 219 input/output pairs was meticulously compiled for training. The inputs were defined by the resonance frequencies f_1 and f_2 in conjunction with the substrate height (H_{sub}). The corresponding outputs encompassed the dimensions of key antenna components, including slot dimensions (R_s, L_{s1}, L_{s2}, W_s, L_{sg}, and W_{sg}), as well as the radius of the patch (R_p) as presented in Figure 3. The training process was focused on optimizing the network's configuration through systematic adjustments to the number of deep layers, the quantity of neurons within each layer, and the implementation of various training algorithms. This iterative approach aimed to automatically fine-tune the weights and biases, ensuring that the output of the ANN closely matched the dual-band antenna's required values and dimensions.

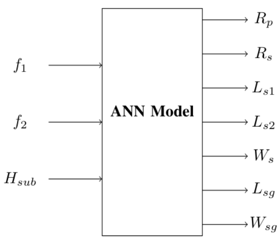

Figure 3. Architecture of the proffered MLP model

The performance of the model is meticulously assessed utilizing statistical metrics like mean absolute error (MAE), mean square error (MSE), and root mean squared error (RMSE). To pinpoint the utmost effective neural network algorithm and reduce the gap amongst target and predicted outcomes, the MLP network undergoes training with an array of algorithms, including RP, CGP, OSS, SCG, CGB, BR, CGF, and LM. Statistics criterion for every learning algorithm presented in Table 2, serve as a measure of the ANN structure's effectiveness. Notably, the BR training algorithm demonstrates the highest precision in aligning desired data and output data, outperforming other alternatives. As a result of its superior performance, the BR training algorithm is selected for our study.

Table 2. Metric measurements used as statistical criterion for various training algorithms

Training algorithm	Training error			Testing error		
	MSE	MAE	$RMSE$	MSE	MAE	$RMSE$
LM	0.0084	0.0605	0.0919	0.0216	0.1206	0.1469
RP	0.0096	0.0696	0.0980	0.0124	0.0898	0.1113
OSS	0.0140	0.0824	0.1182	0.0177	0.0992	0.1329
CGB	0.0102	0.0720	0.1008	0.0128	0.0913	0.1131
SCG	0.0086	0.0676	0.0929	0.0109	0.0886	0.1044
CGF	0.0090	0.0632	0.0951	0.0115	0.0894	0.1073
CGP	0.0176	0.0846	0.1326	0.0094	0.0799	0.0968
BR	0.0030	0.0364	0.0552	0.0085	0.0690	0.0920

The same process used to identify the right training algorithm was used to determine the optimal transfer function for the ANN structure. According to the results in Table 3, the hyperbolic tangent sigmoid (tansig) is the best transfer function for training the MLP network in the hidden layer. The tangent sigmoid transfer function was chosen because of its ability to achieve a low error, as demonstrated by the findings.

The errors associated with varying the number of hidden layers are presented in Table 4, revealing that the best results are achieved with two hidden layers. Numerous experiments were conducted, exploring diverse quantities of neurons in the hidden layers to determine the optimal configuration for training the ANN model. Through these tests, it was observed that employing 30 neurons produced the most favorable outcomes, as evidenced in Table 5. Additionally, the diverse parameters selected for training our ANN structures are succinctly outlined in Table 6.

Table 3. Numeric representations of statistical criteria related to various transfer functions

Transfer function	Training error			Testing error		
	MSE	MAE	RMSE	MSE	MAE	RMSE
Tansig	0.0030	0.0364	0.0552	0.0085	0.0690	0.0920
Satlin	0.0076	0.0622	0.0873	0.0097	0.0813	0.0987
Purelin	0.0073	0.0488	0.0853	0.0101	0.0765	0.1006
Hardlim	0.0076	0.0605	0.0872	0.0081	0.0704	0.0899
Logsig	0.0065	0.0440	0.0805	0.0124	0.0840	0.1115

Table 4. Numeric values indicate the statistical standards across varied number of hidden layers

Number of hidden layers	Training error			Testing error		
	MSE	MAE	RMSE	MSE	MAE	RMSE
1	0.0056	0.0517	0.0750	0.0071	0.0670	0.0840
2	0.0030	0.0364	0.0552	0.0085	0.0690	0.0920
3	0.0706	0.2137	0.2658	0.0706	0.2277	0.2658
4	0.0706	0.2131	0.2656	0.0715	0.2293	0.2673
5	0.0705	0.2116	0.2656	0.0747	0.2350	0.2733

Table 5. Numeric values indicate statistical indicators across varying numbers of neurons in deep layers

Number of neurons	Training error			Testing error		
	MSE	MAE	RMSE	MSE	MAE	RMSE
5	0.0044	0.0463	0.0664	0.0122	0.0864	0.1107
10	0.0046	0.0366	0.0681	0.0137	0.0909	0.1172
15	0.0038	0.0348	0.0618	0.0205	0.0905	0.1431
20	0.0054	0.0333	0.0735	0.0208	0.0983	0.1441
25	0.0030	0.0347	0.0548	0.0161	0.0894	0.1269
30	0.0030	0.0364	0.0552	0.0085	0.0690	0.0920
35	0.0034	0.0379	0.0586	0.0111	0.0767	0.1055
40	0.0073	0.0408	0.0857	0.0100	0.0749	0.1002
50	0.0052	0.0359	0.0724	0.0075	0.0637	0.0866
60	0.0114	0.0738	0.1067	0.0093	0.0840	0.0963

Table 6. Final configuration of the MLP model

Parameter	Attributes
Number of samples	219
Training algorithm	BR
Transfer function	Tansig
Network structure	3-30-30-6

The yardstick for assessing the efficacy of the proffered ANN model is the regression coefficient, which elucidates the correlation among the forecasted values and the intended values. The outcomes for the proposed ANN model in this study are depicted in Figure 4. Across all datasets, the fit is notably satisfactory, with an R-value of 1. Concerning this coefficient, it is evident that the developed ANN model, structured as (3-30-30-6), demonstrates effectiveness in forecasting the values of the dimensions of the suggested antenna.

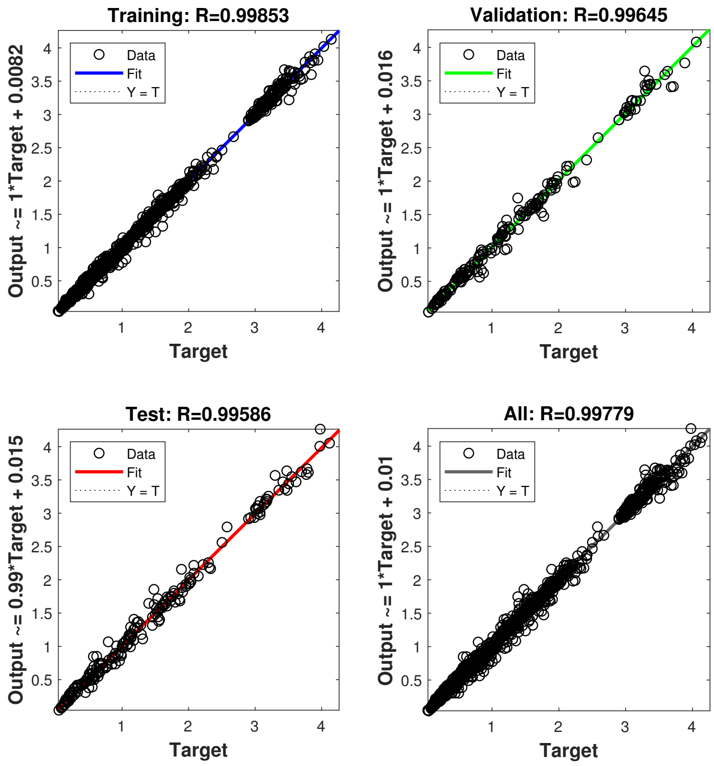

Figure 4. Regression coefficient of developed ANN model

2.4. Results and discussions

Using the developed ANN model, we forecast the dimensions of the antenna engineered for resonance at both 28 GHz and 38 GHz. The resultant outcomes are detailed in Table 7. This table presents the predicted values for key parameters such as R_p, R_s, L_{s1}, L_{s2}, W_s, L_{sg}, and W_{sg}, essential for the optimal performance of the proposed antenna.

Table 7. Predicted dimensions of the proposed antenna

Parameter	R_p	R_s	L_{s1}	L_{s2}	W_s	L_{sg}	W_{sg}
Value (mm)	1.4872	0.7239	1.4876	1.886	0.1986	3.0862	0.4047

The suggested antenna underwent simulation using both HFSS and CST simulators, employing dimensions predicted by the ANN model. A comprehensive analysis of various parameters was conducted to evaluate the antenna's performance. As stated in Figure 5(a), the reflection coefficient of the dual-band antenna was determined through HFSS and CST software. The curves illustrate resonant frequencies at 28.2 GHz and 38 GHz for HFSS and 28 GHz and 38 GHz for CST, with reflection coefficients of -30 dB at the two resonance frequencies for HFSS and -45 dB and -48 dB, respectively, for CST. Notably, the antenna exhibits a significant bandwidth of 4.5 GHz for HFSS and 4 GHz for CST at the first resonance frequency, along with 2.4 GHz for both figures obtained from the two software. Figure 5(b) illustrates the voltage standing wave ratio (VSWR) of the suggested antenna. It is evident that the VSWR remains between 1 and 2 in both operational bands, indicating a well-matched antenna with the transmission line. Moreover, the results obtained from HFSS and CST simulations demonstrate consistencyc, with minor variations attributed to the distinct techniques employed by the two software platforms.

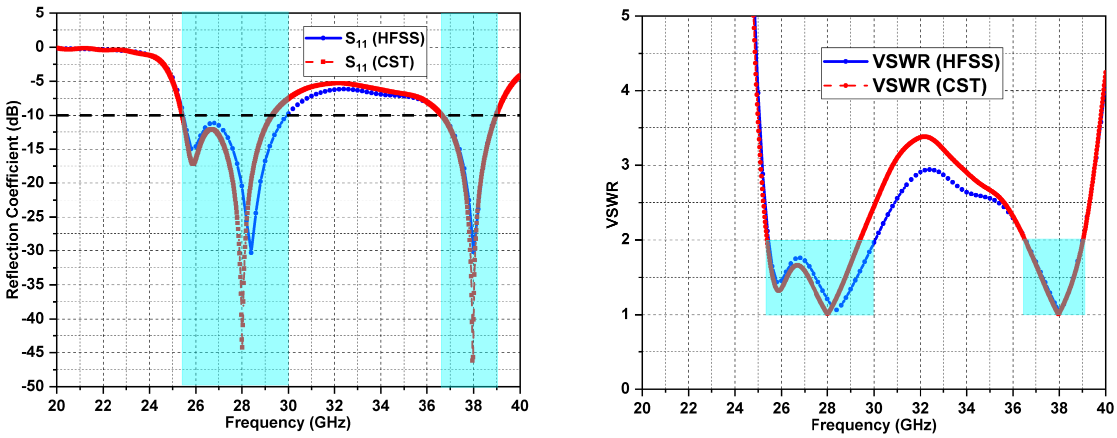

(a) (b)

Figure 5. Electrical properties of the proffered antenna: (a) S_{11} and (b) VSWR

Figure 6 displays the electromagnetic radiation characteristics of the designed antenna layout. In Figures 6(a) and (b), the radiation patterns in the E-plane and H-plane are portrayed in two dimensions, corresponding to resonance frequencies of 28 GHz and 38 GHz. The proffered antenna showcases favorable radiation characteristics in both observation planes. Noteworthy is the fact that at 28 GHz, the antenna exhibits bidirectional and omnidirectional radiation patterns in the H and E planes, respectively. Similarly, at 38 GHz, the antenna demonstrates nearly omnidirectional radiation patterns in both planes. Figure 6(c) displays gain and radiation efficiency across varying frequencies. Notably, exceptional radiation properties are noticed across the full functional bandwidth, with the gain peaking at 4.8 dB and 6.75 dB in the respective frequency bands. Furthermore, the radiation efficiency exceeds 99% in both frequency bands.

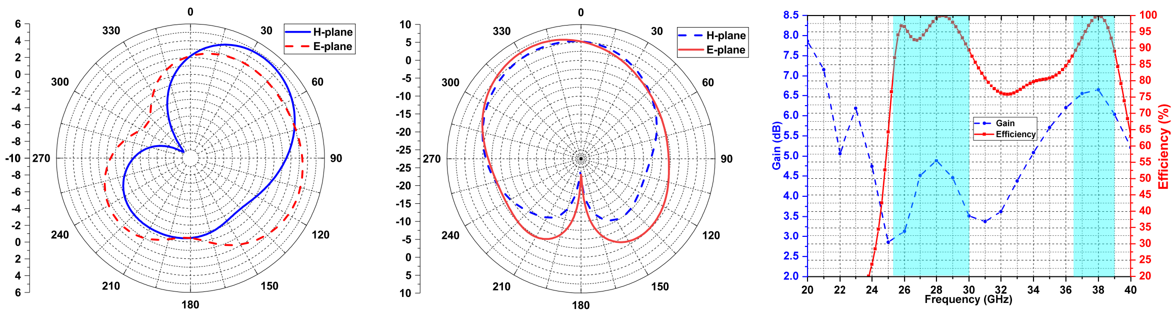

(a) (b) (c)

Figure 6. Proposed antenna radiation characteristics: (a) radiation pattern at 28 GHz, (b) radiation pattern at 38 GHz, and (c) gain and efficiency over frequency

3. DESIGN OF THE PROFFERED MIMO ANTENNA

3.1. Suggested layout and S-parameters

Recognizing the crucial importance of MIMO antennas in exploiting the capabilities of 5G technology, particularly in boosting data rate reliability, this section is devoted to proposing an enhanced MIMO system that goes beyond the single antenna mentioned previously. As depicted in Figures 7(a) and (b), the MIMO configuration consists of four instances of the single antenna strategically arranged orthogonally on the substrate, resulting in a collective footprint measuring $L \times L$ mm^2 (L=16 mm). This orthogonal placement introduces polarization diversity, thereby enhancing isolation. To further bolster the isolation amongst the elements of the MIMO antenna, an isolation structure, comprising four stubs with the same length of L_1=6.5 mm and cross-shaped stubs with a length of L_2=5.5 mm, has been integrated into the top and back sides of the antenna. According to Figures 8(a) and (b), integrating the MIMO setup maintains the individual performance of each element without compromise. Each of the four elements demonstrates impressive performance concerning reflection coefficient and mutual coupling. The operational band covers a range from 25.2 GHz to 29.8 GHz in the initial frequency band, while the bandwidth expands from 36.2 GHz to 38.8 GHz in the second band. This arrangement achieves significant isolation, exceeding 23 dB and 30 dB in the first and higher bands, respectively.

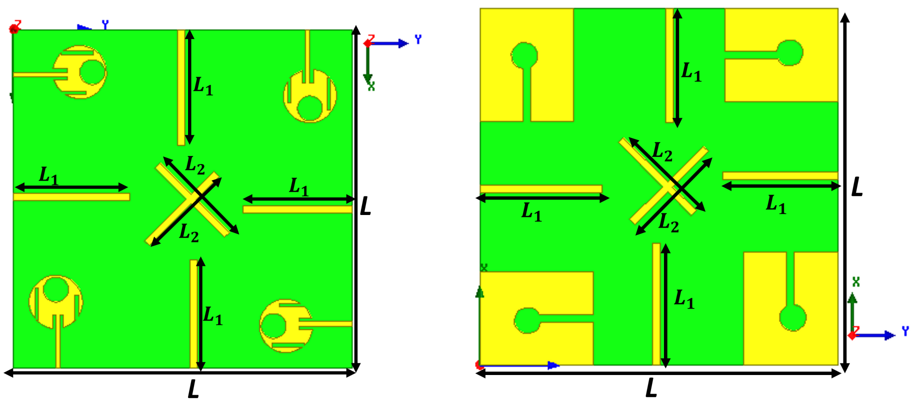

(a) (b)

Figure 7. Layout of the proffered MIMO antenna: (a) top view and (b) back view

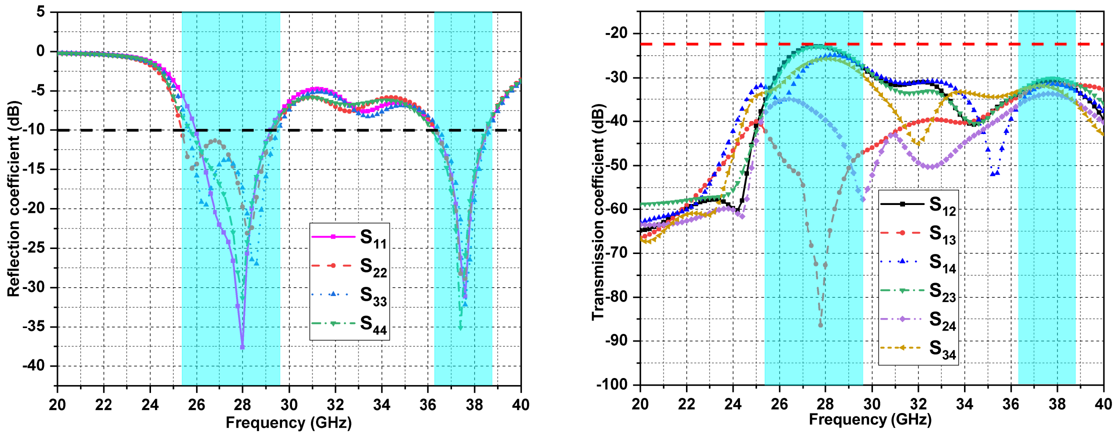

(a) (b)

Figure 8. S-parameter analysis of the proffered 4×4 MIMO antenna: (a) reflection coefficient and (b) transmission coefficient

3.2. Radiation pattern

Figure 9 illustrates the two-dimensional radiation properties of the proposed MIMO antenna across primary planes at frequencies of 28 GHz and 38 GHz. In Figure 9(a), the MIMO antenna displays a double-directional radiation pattern in both the E-plane and H-plane at 28 GHz. Conversely, Figure 9(b) indicates that at 38 GHz, the MIMO antenna emits a predominantly omnidirectional radiation pattern in both planes. This observation suggests that the antenna's radiation traits adapt with frequency, displaying directional tendencies at lower resonance frequencies and transitioning to more uniform radiation at higher resonance frequencies. Additionally, Figure 10 showcases the three-dimensional radiation pattern at 28 GHz in Figure 10(a) and 38 GHz in Figure 10(b), further highlighting the advantageous radiation characteristics of the MIMO antenna. Moreover, the profered MIMO antenna demonstrates maximum gains of 6.84 dB and 7.33 dB at the respective resonance frequencies.

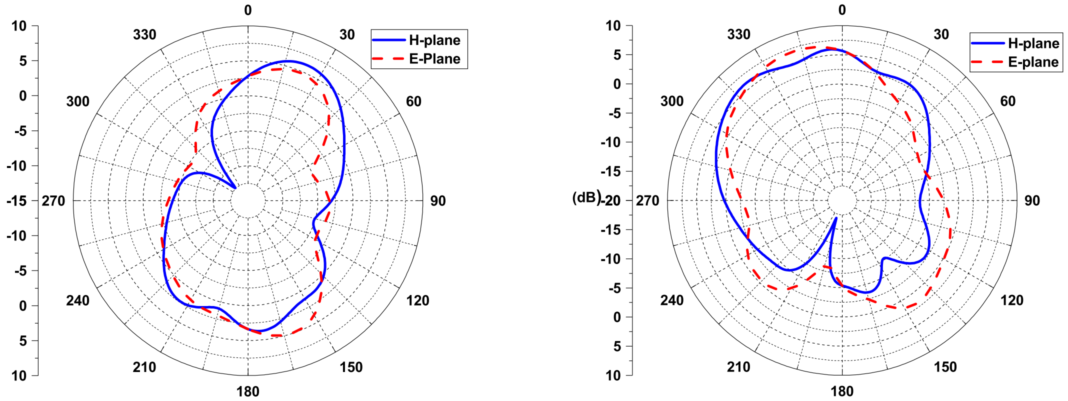

(a) (b)

Figure 9. 2D radiation pattern observed at: (a) 28 GHz and (b) 38 GHz

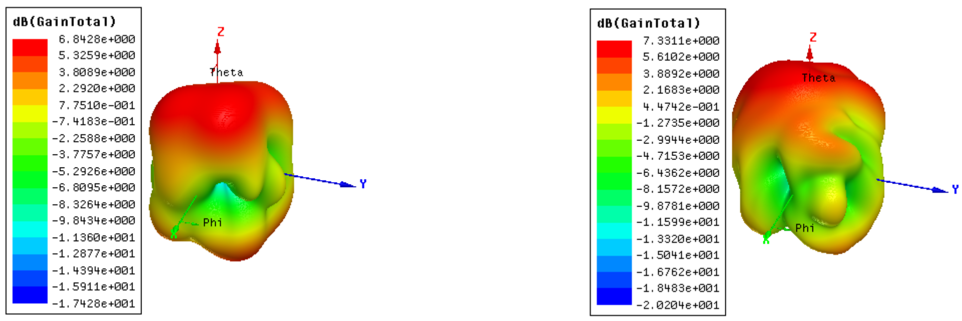

(a) (b)

Figure 10. 3D radiation pattern at: (a) 28 GHz and (b) 38 GHz

3.3. Diversity performance

To thoroughly evaluate the proffered MIMO antenna, an extensive examination of its diversity performance has been carried out, concentrating on vital parameters include the envelope correlation coefficient (ECC) and diversity gain (DG). The ECC acts as an indicator of the independence between the radiation patterns of two antennas, with a lower ECC indicating more distinguishable patterns. According to industry norms, an ECC of 0.5 is considered satisfactory. The ECC for a two-port MIMO antenna can be determined through two approaches: utilizing S-parameters and scrutinizing 3D radiation patterns. By leveraging S-parameters, the ECC is calculated using (1) [24], [25]. In Figure 11, the ECC values for the proposed 4×4 MIMO antenna are depicted, disclosing ECC values below 0.05 in both operational frequency bands.

$$ECC_{ij} = \frac{|S_{ii}^{*}S_{ij} + S_{ji}^{*}S_{jj}|^2}{(1 - (|S_{ii}|^2 + |S_{ji}|^2))\,(-\,(|S_{jj}|^2 + |S_{ij}|^2))} \tag{1}$$

The evaluation of any MIMO system is based on the DG, a key indicator of the reliability and quality of a MIMO antenna in wireless systems. DG can be computed using ECC, as detailed in (2) [26]. Figure 11 illustrates that DG consistently hovers around 10 dB across the operational bands, confirming the antenna's strong performance in terms of diversity.

$$DG_{ij} = 10 \times \sqrt{1 - |ECC_{ij}|^2} \tag{2}$$

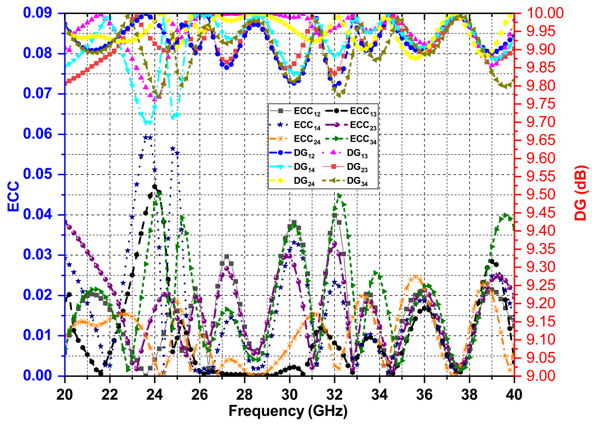

Figure 11. ECC and DG vs frequency of the proffered MIMO antenna

4. COMPARISON WITH SOME RELEVANT RESEARCH

Table 8 provides a comprehensive comparison of the proffered 4×4 MIMO antenna with other dual-band circular patch designs. Notably, the antenna in this study exhibits significant advancements. Its compact size of 16×16×0.8 mm^3 effectively addresses space constraints, marking a notable improvement over larger dimensions in previous designs. Operating at 28/38 GHz, the antenna achieves remarkable bandwidths of 4.5 GHz and 2.4 GHz, demonstrating superior frequency coverage compared to counterparts. With a maximum gain of 7.33 dB, the antenna excels in signal amplification, showcasing competitive performance in this aspect. Efficient isolation (>23 dB and >30 dB at respective bands) minimizes interference between elements, enhancing overall system reliability. Furthermore, the antenna's favorable ECC/DG values (<0.025 and >9.95) underscore its improved performance in terms of ECC and DG. This comprehensive analysis positions the proffered MIMO antenna as a significant advancement in the realm of dual-band circular patch designs, offering enhanced size efficiency, frequency coverage, and overall performance.

Table 8. Comparison of the performance of the proffered MIMO antenna to previous studies

Ref.	Size (mm^3)	Number of elements	Resonance frequency (GHz)	BW (GHz)	Max. Gain (dB)	Isolation (dB)	ECC/DG (dB)
[10]	41.5×10×0.8	4	28/38	1.39/3.33	5.7	>25/25<	<0.001/>9.96
[11]	55×110×0.5	4	28/38	1.06/1.43	8.2	>26/28.32<	<0.001/NA
[12]	20×24×0.508	4	28/38	1/1.2	7.9	>25/26<	<0.001/NA
[13]	79.4×9.65×0.25	4	28/38	3.42/1.45	9	>30/30<	<0.0008/9.99
[14]	33×27.5×0.76	2	28	0.4	6.9	>25	0.001/9.99
This work	16×16×0.8	4	28/38	4.5/2.4	7.33	>23/30<	<0.025/9.95

5. CONCLUSION

This paper presents an innovative dual-band 4×4 circular MIMO antenna explicitly designed for 5G applications. The design methodology is based on ANN to accurately predict the dimensions of the slots inserted in the radiation patch of the proffered single antenna. Four duplicates of the individual antenna are then used to build the 4×4 MIMO configuration. The proffered antenna features not only a compact form factor, but also significant bandwidth in both frequency bands and high gain, making it a robust and competitive candidate for 5G applications, particularly for operation at 28/38 GHz. The integration of ANN into the design process not only speeds up the prediction of dimensions, but also highlights the paper's innovative methodology for optimizing the performance of MIMO antennas. This study represents a substantial contribution to the ongoing advancement of antenna technology for 5G communication systems, presenting a promising solution that seamlessly combines compact design, high bandwidth and increased gain for superior connectivity in the era of next-generation wireless networks.

REFERENCES

[1] A. A. A. Solyman and K. Yahya, "Evolution of wireless communication networks: from 1G to 6G and future perspective," *International Journal of Electrical and Computer Engineering*, vol. 12, no. 4, pp. 3943-3950, 2022, doi: 10.11591/ijece.v12i4.pp3943-3950.

[2] J. Li, Y. Niu, H. Wu, B. Ai, S. Chen, Z. Feng, Z. Zhong, and N. Wang, "Mobility Support for Millimeter Wave Communications: Opportunities and Challenges," *IEEE Communications Surveys & Tutorials*, vol. 24, no. 3, pp. 1816–1842, 2022, doi: 10.1109/COMST.2022.3176802.

[3] P. Loktongbam, D. Pal, A. Bandyopadhyay, and C. Koley, "A brief review on mm-Wave antennas for 5G and beyond applications," *IETE Technical Review*, vol. 40, no. 3, pp. 397–422, 2023, doi: 10.1080/02564602.2022.2121771.

[4] L. Sellak, A. Khabba, S. Chabaa, S. Ibnyaich, A. Sarosh, A. Zeroual, and A. Baddou, "ANFIS-Based 4× 4 Dual Band Circular MIMO Antenna Design with Pretty-Small Size and Large Bandwidth for 5 G Millimeter-Wave Applications at 28/38 GHz," *Journal of Infrared, Millimeter, and Terahertz Waves*, vol. 44, no. 7-8, pp. 551–601, 2023, doi: 10.1007/s10762-023-00924-3.

[5] H. Askari, N. Hussain, M. A. Sufian, S. M. Lee, and N. Kim, "A wideband circularly polarized magnetoelectric dipole antenna for 5G millimeter-wave communications," *Sensors*, vol. 22, no. 6, p. 2338, 2022, doi: 10.3390/s22062338.

[6] S. Ramanathan and A. B. Maria, "A compact four-element MIMO antenna for 5 G millimeter-wave (37–39 GHz) applications," *Journal of Infrared, Millimeter, and Terahertz Waves*, vol. 45, no. 7–8, pp. 604–620, 2024, doi: 10.1007/s10762-024-00990-1.

[7] A. Khabba, J. Amadid, S. Ibnyaich, and A. Zeroual, "Pretty-small four-port dual-wideband 28/38 GHz MIMO antenna with robust isolation and high diversity performance for millimeter-wave 5G wireless systems," *Analog Integrated Circuits and Signal Processing*, vol. 112, no. 1, pp. 83–102, 2022, doi: 10.1007/s10470-022-02045-8.

[8] Z. Xu, *World Of 5g, The-Volume 4: Intelligent Transportation*. World Scientific, 2022.

[9] S. H. Kiani, H. S. Savci, M. E. Munir, A. Sedik, and H. Mostafa, "An Ultra-Wide Band MIMO Antenna System with Enhanced Isolation for Microwave Imaging Applications," *Micromachines*, vol. 14, no. 9, p. 1732, 2023, doi: 10.3390/mi14091732.

[10] U. Rafique, S. Agarwal, N. Nauman, H. Khalil, and K. Ullah, "Inset-fed planar antenna array for dual-band 5G MIMO applications," *Progress In Electromagnetics Research C*, vol. 112, pp. 83–98, 2021, doi: 10.2528/PIERC21021302.

[11] H. M. Marzouk, M. I. Ahmed, and A. H. A. Shaalan, "Novel dual-band 28/38 GHz MIMO antennas for 5G mobile applications," *Progress In Electromagnetics Research C*, vol. 93, pp. 103–117, 2019, doi: 10.2528/PIERC19032303.

[12] K. Raheel, A. Altaf, A. Waheed, S. H. Kiani, D. A. Sehrai, F. Tubbal, and R. Raad, "E-shaped H-slotted dual band mmWave antenna for 5G technology," *Electronics*, vol. 10, no. 9, p. 1019, 2021, doi: 10.3390/electronics10091019.

[13] A. E. Farahat and K. F. Hussein, "Dual-band (28/38 GHz) MIMO antenna system for 5G mobile communications with efficient DoA estimation algorithm in noisy channels," *The Applied Computational Electromagnetics Society Journal (ACES)*, vol. 36, no. 3, pp. 282–294, 2021, doi: 10.47037/2020.ACES.J.360308.

[14] M. Usman, E. Kobal, J. Nasir, Y. Zhu, C. Yu, and A. Zhu, "Compact SIW fed dual-port single element annular slot MIMO antenna for 5G mmWave applications," *IEEE Access*, vol. 9, pp. 91 995–92 002, 2021, doi: 10.1109/ACCESS.2021.3091835.

[15] L. Sellak, L. Aguni, S. Chabaa, S. Ibnyaich, A. Zeroual, and A. Baddou, "Modeling and Designing of a Compact Single Band PIFA Antenna for Wireless Application Using Artificial Neural Network," *Wireless Personal Communications*, vol. 127, no. 4, pp. 3097–3117, 2022, doi: 10.1007/s11277-022-09912-7.

[16] L. Aguni, A. El Yassini, S. Chabaa, S. Ibnyaich, and A. Zeroual, "Design of a symmetric CPW-fed patch antenna for WLAN/WIMAX applications using ANN," *Wireless Personal Communications*, vol. 115, no. 1, pp. 439–456, 2020, doi: 10.1007/s11277-020-07580-z.

[17] S. Ara and P. K. Nunna, "Gain and radiation pattern enhancement using ANN-based reflector antenna for full 5G Sub-6GHz applications," *International Journal of Advanced Technology and Engineering Exploration*, vol. 11, no. 114, pp. 644–667, 2024, doi: 10.19101/IJATEE.2023.10101979.

[18] M. Wang, S. Yang, S. Wu, and F. Luo, "A RBFNN approach for DoA estimation of ultra wideband antenna array," *Neurocomputing*, vol. 71, no. 4-6, pp. 631–640, 2008, doi: 10.1016/j.neucom.2007.08.023.

[19] J. Dong, Y. Li, and M. Wang, "Fast multi-objective antenna optimization based on RBF neural network surrogate model optimized by improved PSO algorithm," *Applied Sciences*, vol. 9, no. 13, p. 2589, 2019, doi: 10.3390/app9132589.

[20] M. Aneesh, J. Ansari, A. Singh, S. Verma, "RBF neural network modeling of rectangular microstrip patch antenna," in *2012 Third International Conference on Computer and Communication Technology*, IEEE, 2012, pp. 241–244, doi: 10.1109/ICCCT.2012.56.

[21] L. Sellak, A. Khabba, S. Chabaa, S. Ibnyaich, A. Baddou, and A. Zeroual, "Adaptive Neuro-Fuzzy Inference System-Based Approach to Design a Multi-Band PIFA Antenna for Wireless Applications," in *2023 IEEE 3rd International Maghreb Meeting of the Conference on Sciences and Techniques of Automatic Control and Computer Engineering (MI-STA)*, IEEE, 2023, pp. 732–737, doi: 10.1109/MI-STA57575.2023.10169336.

[22] S. Ansari, K. A. Alnajjar, S. Abdallah, M. Saad, and A. A. El-Moursy, "Parameter tuning of MLP, RBF, and ANFIS models using genetic algorithm in modeling and classification applications," *International Conference on Information Technology (ICIT)*,

pp. 660–666, 2021, doi: 10.1109/ICIT52682.2021.9491682.

[23] Y. I. Arshavsky, “Neurons versus Networks: The Interplay between Individual Neurons and Neural Networks in Cognitive Functions,” *Neuroscientist*, vol. 23, no. 4, pp. 341–355, 2017, doi: 10.1177/1073858416670124.

[24] K. S. Muttair, O. A. Shareef, and H. B. Taher, “Novel fractal geometry of 4× 4 multi-input and multi-output array antenna for 6G wireless systems,” *TELKOMNIKA (Telecommunication Computing Electronics and Control)*, vol. 22, no. 1, pp. 17–25, 2023, doi: 10.12928/telkomnika.v22i1.24978 Refbacks.

[25] G. Varshney, S. Gotra, V. S. Pandey, and R. S. Yaduvanshi, “Proximity-coupled two-port multi-input-multi-output graphene antenna with pattern diversity for THz applications,” *Nano Communication Networks*, vol. 21, p. 100246, Sep. 2019, doi: 10.1016/j.nancom.2019.05.003.

[26] V. N. K. R. Devana, N. Radha, P. Sunitha, F. N. Alsunaydih, F. Alsaleem, and K. Alhassoon, “Compact MIMO UWB antenna integration with Ku band for advanced wireless communication applications,” *Heliyon*, vol. 10, no. 5, p. e27393, 2024, doi: 10.1016/j.heliyon.2024.e27393.

BIOGRAPHIES OF AUTHORS

Lahcen Sellak received his Bachelor’s degree in Physics from the Ibn Zohr University, Agadir, Morocco and his Master’s degree in Computer Control, Signals and Industrial Systems from Faculty of Sciences Semlalia, Cadi Ayyad University, Marrakech, Morocco in 2017 and 2019, respectively. Currently, he is actively pursuing a Ph.D. degree in Electronics, Telecommunications and Artificial Intelligence at the National School of Applied Sciences, Ibn Zohr University. His research interests include 5G antennas, microwave/millimeter antennas, array antennas, MIMO antennas and the application of artificial intelligence techniques. He can be contacted at email: lahcensellak17@gmail.com.

Asma Khabba received the B.S. in Physics and the Master degree in Control, Industrial Computing, Signals and Systems in 2015 and 2017 respectively from Cadi Ayyad University. She is currently pursuing her studies to accomplish the Ph.D. degree in Telecommunication and Signal Processing at Cady Ayyad University, Marrakech, Morocco. Her research interests include‘ 5G antenna, microwave/millimeter wave antenna, phased array, and MIMO antenna. She can be contacted at email: asma.khabba@edu.uca.ac.ma.

Samira Chabaa is a Professor in the Industrial Department at the National School of Applied Sciences, Ibn Zohr university. She received the Bachelor of Sciences in Electronic Engineering from Moulay Ismail University, Errachidia Morocco. Received the M.A in Electrical Engineering, Power Electronics and Industrial Control, and the Ph.D. degree in Telecommunication and Computing from the Faculty of Science Semlalia, Cadi Ayyad University; Marrakesh Morocco respectively in 2005 and 2011. Reviewer in many international journals. She is currently a co-supervisor of many research works. She has published more than 10 papers in international journals and more than 30 papers in international conferences. Her research interest includes communications and signal processing, time series analysis, linear and nonlinear system identification, and artificial intelligence techniques. She can be contacted at email: s.chabaa@uiz.ac.ma.

Saida Ibnyaich is a professor in the Department of Physics at the Faculty of Sciences Semlalia, Cadi Ayyad University, Marrakesh, Morocco. She received a technical University degree in 1998 from the Higher School of Technology Oujda, Morocco. In 2002 she received a Bachelor degree in Technical Sciences from the Faculty of Sciences and Technology Gueliz, Marrakesh, Morocco. In 2005 She has also received the M.A in Electrical Engineering, Power Electronics and Industrial Control from the Faculy of Science Semlalia, Marrakech, Morocco. In 2013 she received the Ph.D. degree in Telecommunication and Computing from the Faculy of Sciences Semlalia. Her research interest includes telecommunications, microwaves, millimeter waves, and antennas. She can be contacted at email: ibnyaichsaida@gmail.com.

Athmane Baddou was born in 1967 in Ksiba (Beni Mellel), Morocco. He received his DES degree in 1996 and his Doctorat d'Etat degree in 2002 from Cadi Ayyad University, Marrakech, Morocco, both in Automatic Control. Since 2003, he integrated the National School of Applied Sciences (ENSA) Ibn Zohr University, Agadir, as Assistant Professor in the Department on Industrial Engineering. From 2011 to 2019, hi was Deputy Director of ENSA and since 2016, he is Professor in the same department. His main research interests are the constrained control. He can be contacted at email: a.baddou@uiz.ac.ma.

Abdelouhab Zeroual is a professor of Signal Processing and Telecommunication Systems and the Head of Instrumentation, Signals and Systems Laboratory at the Faculty of Sciences Semlalia, Cadi Ayyad University, Marrakesh, Morocco. Received the B.Sc. degree in Physics in 1984, M.Sc. degree in 1986, Diploma of Advanced Studies in 1988 and Ph.D. degree in 1995 from Cadi Ayyad University, Morocco. Reviewer in many international journals and he is currently a supervisor of several research works. His research interest includes solar energy instrumentation, wireless communications and signal processing. He has published more than 60 journal papers and more than 140 conference papers. His current research topics focus on transmitter and receiver diversity techniques for single and multi-user fading communication channels, and wide-band wireless communication systems. He can be contacted at email: zeroual@uca.ac.ma.

Tole Sutikno is a professor in Electrical Engineering Department at the Universitas Ahmad Dahlan (UAD), Yogyakarta, Indonesia. He received his B.Eng., M.Eng., and Ph.D. degrees in Electrical Engineering from Universitas Diponegoro, Universitas Gadjah Mada and Universiti Teknologi Malaysia, in 1999, 2004, and 2016, respectively. He has been a Professor in UAD, Yogyakarta, Indonesia since 2023. He is among the top 2% of researchers named by Stanford University and Elsevier BV as the most influential scientists in the world for 2021–present. He is currently an Editor-in-Chief of the TELKOMNIKA and the Head of the Embedded Systems and Power Electronics Research Group (ESPERG). His research interests include the field of digital design, industrial applications, industrial electronics, industrial informatics, power electronics, motor drives, renewable energy, FPGA applications, embedded system, artificial intelligence, intelligent control, information technology, and digital library. He can be contacted at email: tole@te.uad.ac.id.